Dynamic response of cantilevered thin-walled beams to blast and sonic-boom loadings

Liviu Librescu* and Sungsoo Na[1]

Department of Engineering Science and Mechanics, Virginia Polytechnic Institute and State University, Blacksburg, VA 24061-0219, USA

The paper deals with the dynamic response of anisotropic cantilevered thin-walled beams exposed to blast and sonic boom loadings. The structural model used in this study incorporates a number of non-classical effects such as transverse shear and warping inhibition. Moreover, implementation of a specific ply-angle scheme in each constituent lamina results in elastic cross-couplings beneficial from the response behavior point of view. The influence of these effects is highlighted and the efficiency of the tailoring technique toward enhancing the dynamic response to various overpressure signatures is demonstrated.

1. Introduction

The response of elastic structures to time-dependent external excitations, such as sonic boom and blast loadings, is a subject of much interest in the design of aeronautical and space vehicles as well as of marine and terrestrial ones (see, e.g., Crocker [2], Crocker and Hudson [3], and Houlston et al. [7]).

With the advent of high performance composite material structures and their increased use in the aerospace industry and other fields of the advanced technology, there is a need for further studies of the problem of structural response. This is due to the fact that the new composite material structures exhibit distinguishing features as compared to their metallic counterparts. For this reason, in order to accurately predict the response behavior of structures made of advanced composite materials, refined structural models have to be used. In particular, transverse shear as well as other non-classical effects must be included in their modeling. To date, investigations of the response to sonic booms and blasts have been applied mainly to flat and curved panels (see, e.g., Birman and Bert [1], Librescu and Nosier [10,11].) In spite of the frequent use of thin-walled cantilevered beams in structures such as airplane wings, helicopter blades, robotic manipulator arms and space booms, very few studies have considered the behavior of *thin-walled anisotropic cantilevers* subjected to time-dependent external excitations. In this connection the reader is referred to the paper by Song and Librescu [18] where, pertinent references to the literature in this area can be found.

The development of adequate approaches toward the prediction of the response of composite thin-walled beams to time-dependent external pulses is of practical importance as far as safe design is concerned. The present paper is aiming to fill the existing gap in this field and is concerned with two related issues, namely: (i) the development of a powerful mathematical methodology for determining the response of thin-walled cantilevers to time-dependent external excitations, and (ii) the highlight of the influence of the various effects, and specially of the anisotropy, transverse shear and warping inhibition on the dynamic response of thin-walled beam cantilevers.

It should be mentioned that the theory of anisotropic thin-walled beams as used in this paper was developed in the paper by Song and Librescu [17]. However, in order to be reasonably self-contained, a number of basic steps yielding the pertinent governing equations will be displayed.

*Corresponding author. Tel.: +1 540 231-5916; Fax: +1 540 231-4574; E-mail: librescu@vt.edu.

[1]Current address: Department of Automation Engineering, Korea Polytechnic University, Keonghi-do 429-450, Korea.

2. Structural model: Basic equations

The structural model of single-cell thin-walled beams used in this study incorporates a number of non-classical features such as: (i) Anisotropy of constituent material layers; (ii) Transverse shear, (iii) Non-uniform twist, in the sense that the rate of twist $d\Theta/dz$ is no longer assumed to be constant as in the Saint-Venant torsional model, but a function of the spanwise coordinate and (iv) Primary and secondary warping effects.

In accordance with the above statements and in order to reduce the 3D problem to an equivalent 1D one, the components of the displacement vector are expressed as (see Song and Librescu [17]):

$$u(x,y,z,t) = u_0(z,t) - y\Theta(z,t), \tag{1a}$$

$$v(x,y,z,t) = v_0(z,t) + x\Theta(z,t), \tag{1b}$$

$$w(x,y,z,t) = w_0(z,t)$$
$$+ \theta_x(z,t)\left[y(s) - n\frac{dx}{ds}\right]$$
$$+ \theta_y(z,t)\left[x(s) + n\frac{dy}{ds}\right]$$
$$- \Theta'(z,t)[F_\omega(s) + na(s)], \tag{1c}$$

where

$$\theta_x(z,t) = \gamma_{yz}(z,t) - v_0'(z,t), \tag{2a}$$

$$\theta_y(z,t) = \gamma_{xz}(z,t) - u_0'(z,t), \tag{2b}$$

and

$$a(s) = -y(s)\frac{dy}{ds} - x(s)\frac{dx}{ds}. \tag{2c}$$

Here $\theta_x(z,t)$ and $\theta_y(z,t)$ denote the rotations about axes x and y, respectively, Θ the twist about the z-axis, while γ_{yz} and γ_{xz} denote the transverse shear strains in the planes yz and xz, respectively.

In addition,

$$F_\omega(s) = \int_0^s [r_n(s) - \psi]\,ds, \tag{3}$$

plays the role of the primary warping function, $na(s)$ that of the second warping, whereas the torsional function ψ and the quantity $r_n(s)$ are defined as

$$\psi = \frac{\oint_C r_n(s)\dfrac{ds}{h(s)}}{\oint_C \dfrac{ds}{h(s)}}, \tag{4}$$

and

$$r_n(s) = x(s)\frac{dy}{ds} - y(s)\frac{dx}{ds}, \tag{5}$$

respectively.

For more details concerning these quantities see the papers by Song and Librescu [13,17]). Equations (1) and (2) reveal that six kinematic variables: $u_0(z,t)$, $v_0(z,t)$, $w_0(z,t)$, $\theta_x(z,t)$, $\theta_y(z,t)$ and $\Theta(z,t)$ representing three translations in the x, y, z directions and three rotations about the x, y and z axes, respectively, are used to define the displacement vector of components u, v and w in the x, y and z directions, respectively. The quantity $h[\equiv h(s)]$ denotes the wall thickness of the beam (allowed to vary along the periphery); $\oint_C(\cdot)\,ds$ denotes the integral around the entire periphery C of the mid-line cross-section of the beam; while $\int_0^s r_n(s)\,ds$ $[\equiv \Omega(s)]$ is referred to as the sectorial area. For the case of h uniform in the circumferential direction, Eq. (4) reduces to $\psi = 2A_c/\beta$ where A_c denotes the cross-sectional area bounded by the mid-line contour while β denotes the total length of the contour mid-line.

Based on the kinematic representations, Eqs (1) and (2), the strain measures assume the following form (see Song and Librescu [17]):

Axial strain:

$$\varepsilon_{zz}(n,s,z,t) = \overline{\varepsilon}_{zz}(s,z,t) + n\overline{\overline{\varepsilon}}_{zz}(s,z,t), \tag{6a}$$

where

$$\overline{\varepsilon}_{zz}(s,z,t) = w_0'(z,t) + \theta_y'(z,t)x(s)$$
$$+ \theta_x'(z,t)y(s) - \Theta''(z,t)F_\omega(s) \tag{6b}$$

and

$$\overline{\overline{\varepsilon}}_{zz}(s,z,t) = \theta_y'(z,t)\frac{dy}{ds} - \theta_x'(z,t)\frac{dx}{ds}$$
$$- \Theta''(z,t)a(s) \tag{6c}$$

are the axial strains associated with the primary and secondary warping, respectively.

Tangential shear strain:

$$\varepsilon_{sz}(s,z,t) = \overline{\varepsilon}_{sz}(s,z,t) + 2\frac{A_c}{\beta}\Theta'(z,t), \tag{7a}$$

where

$$\overline{\varepsilon}_{sz}(s,z,t) = [\theta_y(z,t) + u_0'(z,t)]\frac{dx}{ds}$$
$$+ [\theta_x(z,t) + v_0'(z,t)]\frac{dy}{ds}. \tag{7b}$$

Transverse shear strain

$$\varepsilon_{nz}(s,z,t) = [\theta_y(z,t) + u_0'(z,t)]\frac{\mathrm{d}y}{\mathrm{d}s}$$

$$- [\theta_x(z,t) + v_0'(z,t)]\frac{\mathrm{d}x}{\mathrm{d}s}. \quad (8)$$

Here, and in the following developments x, y and z is the *global* coordinate system, where the z-axis coincides with the locus of symmetrical points of the cross-sections along the wing-span; n, s, z is a *local* coordinate system, while $(\cdot)' \equiv \partial(\cdot)/\partial z$.

For the problem considered herein, $u_0(z,t)$, $v_0(z,t)$, $w_0(z,t)$, and $\theta_x(z,t)$, $\theta_y(z,t)$ and $\Theta(z,t)$ constitute the basic one-dimensional unknown functions of the problem. When the transverse shear is ignored, $\theta_x \rightarrow -v_0'$ and $\theta_y \rightarrow -u_0'$ and, as a result, the number of unknowns is reduced to only four.

As concerns the 2D constitutive equations, these have been obtained in the paper by Song and Librescu [17] for the case of a beam consisting of N homogeneous anisotropic elastic layers. Upon considering the hoop stress resultant negligibly small when compared to the remaining ones, the constitutive equations can be expressed as:

$$N_{zz}(s,z,t) = K_{11}\overline{\varepsilon}_{zz} + K_{12}\overline{\varepsilon}_{sz}$$
$$+ K_{13}\Theta' + K_{14}\overline{\overline{\varepsilon}}_{zz}, \quad (9a)$$

$$N_{sz}(s,z,t) = K_{21}\overline{\varepsilon}_{zz} + K_{22}\overline{\varepsilon}_{sz}$$
$$+ K_{23}\Theta' + K_{24}\overline{\overline{\varepsilon}}_{zz}, \quad (9b)$$

$$N_{zn}(s,z,t) = A_{44}\varepsilon_{zn}, \quad (9c)$$

$$L_{zz}(s,z,t) = K_{41}\overline{\varepsilon}_{zz} + K_{42}\overline{\varepsilon}_{sz}$$
$$+ K_{43}\Theta' + K_{44}\overline{\overline{\varepsilon}}_{zz}, \quad (9d)$$

$$L_{sz}(s,z,t) = K_{51}\overline{\varepsilon}_{zz} + K_{52}\overline{\varepsilon}_{sz}$$
$$+ K_{53}\Theta' + K_{54}\overline{\overline{\varepsilon}}_{zz}, \quad (9e)$$

In Eqs (9a)–(9e) N_{zz} and N_{sz} denote the tangential stress-resultants, N_{zn} denotes the transverse shear stress-resultant, L_{zz} and L_{sz} denote the stress-couples; while K_{ij} denote the modified local stiffness coefficients listed in Appendix A.

3. The governing system

Consistent with the kinematical equations, Eqs (1a) to (1c), the 1D version of the equations of motion and the associated boundary conditions can be obtained by means of Hamilton's variational principle.

Employment in the obtained equations of motion (not displayed here) of constitutive equations, Eqs (9a)–(9e), and of strain-displacement relations, Eqs (6)–(8), results in the 1D variant of the governing equations.

These equations feature a full coupling among the various elastic modes, i.e., among extension, twist, transversal bending (flapping), lateral-bending (lagging) and transverse shear. However, as it was revealed, in a number of recent works, (see, e.g., Weisshaar [19], Librescu and Simovich [9] and Librescu and Thangjitham [12]), flapping-twist cross-coupling turns out to be of an exceptional importance towards the enhancement of the response behavior of aircraft wings.

As it was shown in Rehfield and Atilgan [15] and Smith and Chopra [16], the ply-angle distribution with respect to the spanwise z-axis inducing such a cross-coupling is

$$\theta(y) = -\theta(-y). \quad (10)$$

By considering such a ply-angle scheme the governing equations expressed in terms of displacement quantities are:

$$\delta v_0: \quad a_{55}(v_0'' + \theta_x') + \underline{a_{56}\Theta'''} + p_y = b_1\ddot{v}_0, \quad (11a)$$

$$\delta\theta_x: \quad a_{33}\theta_x'' + a_{37}\Theta'' - a_{55}(v_0' + \theta_x) - \underline{a_{56}\Theta''}$$
$$= (b_4 + b_{14})\ddot{\theta}_x, \quad (11b)$$

$$\delta\Theta: \quad -a_{66}\Theta'''' + a_{77}\Theta''$$
$$\underline{\phantom{-a_{56}}}$$
$$-\underline{a_{56}(v_0''' + \theta_x'')} + a_{73}\theta_x'' + m_z$$
$$= (b_4 + b_5)\ddot{\Theta} - \underline{\underline{(b_{10} + b_{18})\ddot{\Theta}''}}. \quad (11c)$$

For cantilevered beams, the boundary conditions to be prescribed are:
at $z = 0$:

$$v_0 = 0, \quad \theta_x = 0, \quad \Theta = 0, \quad \underline{\Theta' = 0}, \quad (12\text{a–d})$$

and at $z = L$:

$$\delta v_0: \quad a_{55}(v_0' + \theta_x) + \underline{a_{56}\Theta''} = 0, \quad (13a)$$

$$\delta\theta_x: \quad a_{33}\theta_x' + a_{37}\Theta' = 0, \quad (13b)$$

$$\delta\Theta: \quad -a_{66}\Theta''' + a_{77}\Theta' - \underline{a_{56}(v_0'' + \theta_x')}$$
$$+ a_{37}\theta_x' = -\underline{\underline{(b_{10} + b_{18})\ddot{\Theta}'}}, \quad (13c)$$

$$\delta\Theta': \quad a_{56}(v_0' + \theta_x) + \underline{a_{66}\Theta''} = 0. \quad (13d)$$

The terms underscored in Eqs (11)–(13) by single and double dotted lines are associated with the warping inhibition and the warping inertia, respectively, whereas the term underscored by a solid line is associated with the rotatory inertia.

For infinitely rigid in transverse shear beam model, the counterpart of Eqs (11a)–(11c) becomes:

$$\delta v_0: \quad a_{33} v_0^{\mathrm{IV}} - a_{37} \Theta''' + p_y$$
$$= -b_1 \ddot{v}_0 + \underline{(b_4 + b_{14}) \ddot{v}_0''}, \qquad (14\mathrm{a})$$

$$\delta \Theta: \quad -a_{66} \Theta^{\mathrm{IV}} + a_{77} \Theta'' - a_{73} v_0''' + m_z$$
$$= (b_4 + b_5) \ddot{\Theta} - (b_{10} + b_{18}) \ddot{\Theta}'' \quad (14\mathrm{b})$$

while the boundary conditions (12) and (13) become: at $z = 0$:

$$\Theta = \Theta' = v_0 = v_0' = 0, \qquad (15\mathrm{a–d})$$

and at $z = L$:

$$\delta v_0: \quad a_{33} v_0''' = \underline{(b_4 + b_{14}) \ddot{v}_0'}, \qquad (16\mathrm{a})$$

$$\delta v_0': \quad a_{37} \Theta' - a_{33} v_0'' = 0, \qquad (16\mathrm{b})$$

$$\delta \Theta: \quad -a_{66} \Theta''' + a_{77} \Theta' - a_{37} v_0''$$
$$= -(b_{10} + b_{18}) \ddot{\Theta}', \qquad (16\mathrm{c})$$

$$\delta \Theta': \quad \Theta'' = 0. \qquad (16\mathrm{d})$$

From Eqs (11)–(13) is readily seen that in addition to the transverse bending stiffness (a_{33}), twist stiffness (a_{77}) and transverse shear stiffness in the y direction, (a_{55}), the system is governed by the warping stiffness (a_{66}), twist-transverse shear (a_{56}), and bending-twist (a_{37}) cross-couplings. From Eqs (14)–(16) it becomes also evident that for non-shearable beams, the stiffness quantities a_{55} and a_{56} become immaterial.

From the previously displayed equations it also emerges that for both shear deformable beams and their infinitely rigid in transverse shear counterpart, the governing equations exhibit the same order (namely eight), and the same number of boundary conditions (namely four) has to be prescribed at each edge. A similar feature is also valid in the context of the solid beam model (see Karpouzian and Librescu [8]).

In Eqs (11)–(16), the coefficients a_{ij} ($\equiv a_{ji}$) and b_i denote stiffness and inertia quantities. Their expressions are displayed in Appendix. Moreover $p_y(z, t)$ and $m_z(z, t)$ denote the distributed force per unit span

length and the twist moment about the z axis. For the problem at hand, only the distributed force will be considered, implying that in the forthcoming developments $m_z(z, t) = 0$.

4. Time-dependent loads associated with blast and sonic-boom pulses

Herein, the response of thin-walled beams to explosive blast and sonic boom overpressure signatures will be addressed. For the case of blast loadings, various analytical expressions have been proposed and discussed (see, e.g., Houlston et al. [7], Gupta [5], Gupta et al. [6], Birman and Bert [1]). As it was clearly established, the blast wave reaches the peak value in such a short time that the structure can be assumed to be loaded instantly. Based on experimental evidence, it may also be assumed that the pressure is uniformly distributed over the plate. This fact is also assumed in the case of sonic boom pulses. In accordance with above mentioned references, the overpressure associated with the blast pulses can be described in terms of the modified Friedlander exponential decay equation as:

$$p_y(s, z, t)(\equiv p_y(t)) = P_{\mathrm{m}} \left(1 - \frac{t}{t_{\mathrm{p}}}\right) \mathrm{e}^{-a't/t_{\mathrm{p}}}, \qquad (17)$$

where the negative phase of the blast is included. In Eq. (17), P_{m} denotes the peak reflected pressure in excess of the ambient one; t_{p} denotes the positive phase duration of the pulse measured from the time of impact of the structure and a' denotes a decay parameter which has to be adjusted to approximate the overpressure signature from the blast tests. A depiction of the ratio p_y/P_{m} vs. time for various values of the ratio a'/t_{p} and a fixed value of t_{p} is displayed in Fig. 1(a). As it could be inferred, the triangular load may be viewed as a limiting case of Eq. (17), occurring for $a'/t_{\mathrm{p}} \to 0$.

As concerns the sonic-boom loading, this can be modeled as an N-shaped pressure pulse arriving at a normal incidence. Such a pulse corresponds to an idealized far field overpressure produced by an aircraft flying supersonically in the earth's atmosphere or by any supersonic projectile rocket or missile (see Crocker [2] and Gottlieb and Ritzel [4]). The overpressure signature of the N-wave shock pulse can be described by
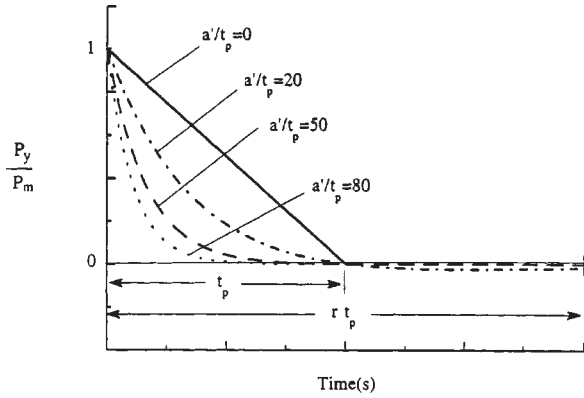
(a)
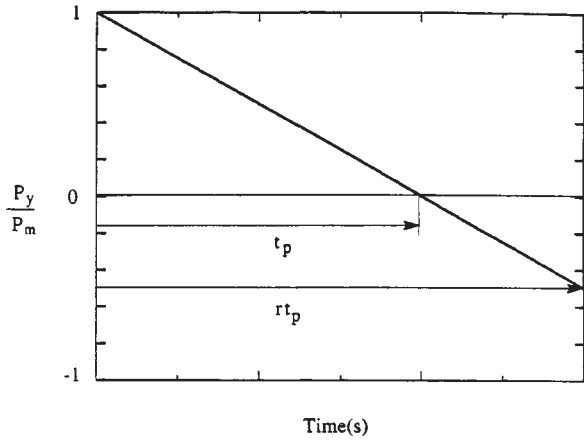
(b)

Fig. 1. Typical pressure time-history. 1(a) Explosive overpressure signature for various values of a'/t_p. Negative phase of the pulse included. 1(b) Sonic-boom overpressure signature.

$$p_y(s, z, t)(\equiv p_y(t))$$

$$= \begin{cases} P_m\left(1 - \dfrac{t}{t_p}\right) & \text{for } 0 < t < rt_p, \\ 0 & \text{for } t < 0 \text{ and } t > rt_p, \end{cases} \quad (18)$$

where r denotes the shock pulse length factor, and P_m and t_p maintain the same meaning as in the case of blast pulses. It may easily be seen that: (i) for $r = 1$ the N-shaped pulse degenerates into a triangular pulse; (ii) for $r = 2$ a symmetric N-shaped pressure pulse is obtained; while (iii) for $1 < r < 2$ the N-shaped pulse becomes an asymmetric one as shown in Fig. 1(b).

Another special case emerging from blast and sonic-boom pulses corresponds to a step pulse. This case is obtained either from Eq. (17), when $t_p \to \infty$, or from Eq. (18) when $r = 1$ and $t_p \to \infty$.

In addition, the cases of the the sine and rectangular pressure pulses described as:

$$p_y(s, z, t) \equiv p_y(t)$$

$$= \begin{cases} P_m \sin \pi t/t_p, & 0 \leqslant t \leqslant t_p, \\ 0, & t > t_p, \end{cases} \right\} \text{sine pulse} \\ P_m, & 0 \leqslant t \leqslant t_p, \\ 0, & t > t_p, \end{cases} \right\} \begin{array}{l} \text{rectangular} \\ \text{pulse} \end{array} \quad (19)$$

will be considered in the study of the dynamic response.

5. Solution methodology

A number of successive steps aiming to derive a solution to the dynamic response problem have to be implemented. As a first step, Hamilton's variational principle stating that

$$\int_{t_1}^{t_2} (\delta T - \delta V + \delta W)\,dt = 0,$$

$$\delta v_0 = \delta \theta_x = \delta \Theta = 0 \quad \text{at} \quad t = t_1, t_2 \quad (20)$$

will be used.

Herein T and V denote the kinetic and strain energies, respectively while W is the work done by the external distributed loads; t_1 and t_2 denote two arbitrary instants of time t while δ denotes the variation operator.

For the problem at hand for which the ply-angle configuration defined by Eq. (10) was adopted, one can express

$$\int_{t_1}^{t_2} \delta T\,dt$$

$$= -\int_{t_1}^{t_2} \int_0^L \left(I_1 \delta v_0 + I_2 \delta \Theta + I_3 \delta \theta_x\right) dt\,dz. \quad (21)$$

where I_i denote inertia terms defined in the papers by Song and Librescu [17,18]

$$\delta V = -\int_0^L \left[(M_x' - Q_y)\delta\theta_x \right.$$

$$+ (B_\omega'' + M_z')\delta\Theta + Q_y'\delta v_0\right] dz$$

$$+ \left[M_x\delta\theta_x - B_\omega\delta\Theta' \right.$$

$$+ (B_\omega' + M_z)\delta\Theta + Q_y\delta v_0\right]\Big|_0^L \quad (22)$$

and

$$\delta W = \int_0^L p_y \delta v_0 \, \mathrm{d}z. \tag{23}$$

From Eq. (20) considered in conjunction with Eqs (21)–(23), with the definitions of 1D stress-resultants Q_y, stress-couples M_x, M_z and biomoment B_ω as (see Librescu and Song [13] and Song and Librescu [17]):

$$Q_y(z,t) = \oint_C \left(N_{sz} \frac{\mathrm{d}y}{\mathrm{d}s} - N_{zn} \frac{\mathrm{d}x}{\mathrm{d}s} \right) \mathrm{d}s,$$

$$M_x(z,t) = \oint_C \left(y N_{zz} - L_{zz} \frac{\mathrm{d}x}{\mathrm{d}s} \right) \mathrm{d}s,$$

$$M_z(z,t) = 2 \oint_C N_{sz} \psi \, \mathrm{d}s,$$

$$B_\omega(z,t) = \oint_C [F_\omega(s) N_{zz} + a(s) L_{zz}] \, \mathrm{d}s \tag{24}$$

and the 2D constitutive equations, Eqs (9a)–(9e), for independent and arbitrary variations $\delta\theta_x$, δv_0 and $\delta\Theta$, from (20), the equations of motion in terms of displacement quantities, as well as the boundary conditions can be obtained. However, in order to implement the Extended Galerkin Method, one uses Eq. (20), which in conjunction with Eqs (21)–(23) can be written in compact form as:

$$\int_{t_1}^{t_2} \left[\int_0^L \big[(11a)\delta v_0 + (11b)\delta\theta_x + (11c)\delta\Theta \big] \, \mathrm{d}z \right.$$
$$+ \big[(13a)\delta v_0 + (13b)\delta\theta_x + (13c)\delta\Theta$$
$$\left. + (13d)\delta\Theta' \big] \Big|_0^L \right] \mathrm{d}t = 0. \tag{25}$$

The numbers in brackets identify the left hand expressions of the equations of motion and boundary conditions at $z = L$, displayed in the paper under the same numbers and modified by passing the left hand side members in the right hand side. Within the second step, for the problem at hand one assumes for the displacement quantities the representation

$$\big[v_0(z,t); \theta_x(z,t); \Theta(z,t) \big]$$
$$= \sum_{j=1}^N \big[v_j(z)q_j(t); w_j(z)q_j(t); W_j(z)q_j(t) \big], \tag{26}$$

where $v_j(z)$, $w_j(z)$ and $W_j(z)$ are the trial functions which have to fulfill all the kinematic boundary conditions and are assumed to be known while $q_j(t)$ are the generalized coordinates whose determination constitutes the central goal of the dynamic response prob-

lem. For the problem at hand the trial functions are represented as polynomials in the Z $(\equiv z/L)$ variable which exactly fulfill the boundary conditions at $Z = 0$. Representations (26) as well as that of the overpressure signatures are replaced in Eq. (25) and the integration with respect to the dimensionless spanwise Z-coordinate is performed. For the present problem the boundary conditions at $Z = 1$ being in general not fulfilled, corrective terms instead of zero-valued ones appear in the process of integration in Eq. (25), terms which compensate for the non-fulfillment of the non-essential boundary conditions. As a result, an equation expressed in matrix form as

$$\boldsymbol{D} = 0 \tag{27}$$

is obtained where

$$\boldsymbol{D} \equiv \boldsymbol{M}\ddot{\boldsymbol{q}} + \boldsymbol{K}\boldsymbol{q} - \boldsymbol{F}. \tag{28}$$

Herein $\boldsymbol{q}$ is a $3N \times 1$ column matrix whose elements are $q_j(t)$; $\boldsymbol{M}$ and $\boldsymbol{K}$ are $3N \times 3N$ square matrices, the latter one containing also the corrective boundary terms, while $\boldsymbol{F}(\equiv \boldsymbol{F}(t))$ is the input $3N \times 1$ column matrix.

Equation

$$\boldsymbol{M}\ddot{\boldsymbol{q}} + \boldsymbol{K}\boldsymbol{q} = \boldsymbol{F} \tag{29}$$

constitutes a set of coupled ordinary differential equations. Multiplying Eq. (29) by $\boldsymbol{M}^{-1}$, introducing the generalized velocities $\dot{\boldsymbol{q}}$ as auxiliary variables by means of the matrix identity $\dot{\boldsymbol{q}} - \dot{\boldsymbol{q}} = \boldsymbol{0}$ and defining the state space vector

$$\boldsymbol{X} = \left\{ \begin{matrix} \boldsymbol{q} \\ \dot{\boldsymbol{q}} \end{matrix} \right\}, \tag{30}$$

one can express Eq. (29) in state space form as:

$$\dot{\boldsymbol{X}} = \boldsymbol{A}\boldsymbol{X} + \boldsymbol{B}\boldsymbol{F}, \tag{31}$$

where

$$\boldsymbol{A} = \left[\begin{array}{c|c} \boldsymbol{0} & \boldsymbol{I} \\ \hline -\boldsymbol{M}^{-1}\boldsymbol{K} & \boldsymbol{0} \end{array} \right],$$

$$\boldsymbol{B} = \left\{ \begin{matrix} \boldsymbol{0} \\ \boldsymbol{M}^{-1} \end{matrix} \right\}. \tag{32}$$

Applying Laplace transform to each side of Eq. (31) yields

$$\overline{\boldsymbol{X}}(s) = (s\boldsymbol{I} - \boldsymbol{A})^{-1}\boldsymbol{X}(0)$$
$$+ (s\boldsymbol{I} - \boldsymbol{A}^{-1})\boldsymbol{B}\overline{\boldsymbol{F}}, \tag{33}$$

where the overbars denote Laplace transforms of the counterpart quantities without the overbar, $\boldsymbol{X}(0)$ de-

notes the initial state vector while s denotes Laplace transform variable.

As a result, the time response $\boldsymbol{X}(t)$ is obtained as the inverse Laplace transform of Eq. (33) as:

$$\boldsymbol{X}(t) = \mathcal{L}^{-1}\{[\phi(s)]\boldsymbol{X}(0)\}$$
$$+ \mathcal{L}^{-1}[\phi(s)\boldsymbol{B}\overline{\boldsymbol{F}}(s)], \qquad (34)$$

where

$$\phi(s) \equiv (s\boldsymbol{I} - \boldsymbol{A})^{-1}, \qquad (35)$$

and $\mathcal{L}^{-1}$ denotes the inverse Laplace transform operation.

In this form the solution for $\boldsymbol{X}(t)$ contains the contributions of initial conditions and of the forcing function.

In the case of zero initial conditions, as is considered in the present numerical illustrations, the solution reads:

$$X_i(t) = \mathcal{L}^{-1}\left\{\frac{Q_i(s)}{g(s)}\right\}$$
$$= \sum_{i=1}^{12} \frac{Q_i(\lambda_i)}{(\mathrm{d}g/\mathrm{d}s)_{s=\lambda_i}}\, e^{\lambda_i t}. \qquad (36)$$

Herein λ_i $(i = \overline{1,12})$ are the roots of the polynomial $g(s)$ which play the role of eigenvalues of the system, while $Q_i(s)$ is a polynomial whose coefficients depend upon the mechanical properties of the structure and on the characteristics of the pressure pulse.

6. Numerical illustrations and discussion

The numerical illustrations concern the dynamic response of a cantilevered thin-walled beam of a bicon-

c = 10 in (0.254 m)
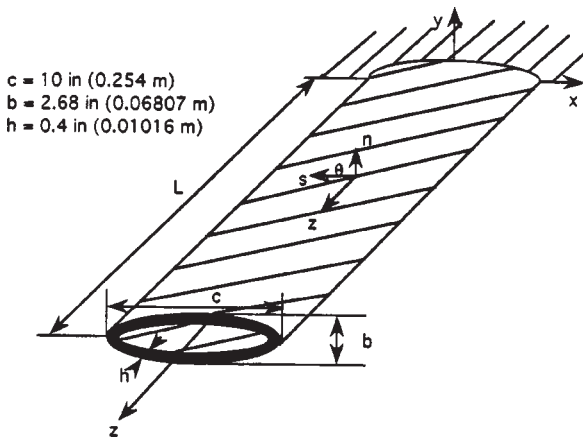b = 2.68 in (0.06807 m)
h = 0.4 in (0.01016 m)

Fig. 2. Geometry of the thin-walled beam.

vex cross-section profile (see Fig. 2). This profile was used in the study of the aeroelastic behavior of high speed wing structures in (see Librescu et al. [14]).

Two materials are considered in the numerical illustrations. One of them is the graphite–epoxy material whose on-axis properties are:

$$E_\mathrm{L} = 30 \times 10^6 \text{ psi } (20.68 \times 10^{10} \text{ N/m}^2)$$

$$E_\mathrm{T} = 0.75 \times 10^6 \text{ psi } (5.17 \times 10^9 \text{ N/m}^2)$$

$$G_\mathrm{LT} = 0.37 \times 10^6 \text{ psi } (2.55 \times 10^9 \text{ N/m}^2)$$

$$G_\mathrm{TT} = 0.45 \times 10^6 \text{ psi } (3.10 \times 10^9 \text{ N/m}^2)$$

$$\mu_\mathrm{TT} = \mu_\mathrm{LT} = 0.25,$$

$$\rho = 14.3 \times 10^{-5} \text{ lb sec}^2/\text{in}^4 (1528.15 \text{ N s}^2/\text{m}^4)$$

where subscripts L and T denote directions parallel and transverse to the fibers, respectively.

The second material has transversely-isotropic properties, the surface of isotropy being parallel at each point to the mid-surface of the beam. Due to its outstanding thermomechanical properties, this material (known as pyrolitic-graphite and its alloys) is a good candidate to be used in the structure of high-speed flight vehicles.

The displayed results correspond to the case of zero initial conditions and of $P_\mathrm{m} = 500$ lb/L. In Figs 3 and 4 the dimensionless deflection $\widetilde{V}(\equiv v_0/L)$ response of the beam tip to a sonic boom overpressure signature is displayed. Figure 3 reveals the efficiency of the tailoring technique to confine the increase of the transverse deflection. From this graph it appears that for $\theta = 90°$, at which the maximum bending stiffness is reached (see Librescu et al. [14]), a minimum deflection throughout the positive and negative phases of the pulse and even in the free motion range (i.e., for $t > rt_\mathrm{p}$, when the wave has left the structure), is reached.

In Figure 4 the effect of the transverse shear flexibility of the material of the structure, measured in terms of the ratio E/G', is highlighted. Herein E and G' denote the tangential Young's modulus and transverse shear modulus, respectively, where $E/G' = 0$ corresponds to the non-shearable (Bernoulli–Euler) beam model. Whereas during the positive and negative phases of the blast, transverse shear has an almost negligible effect on the deflection, in the free motion range its effect is rather strong and it becomes evident that the classical theory inadvertently underestimates the deflection.
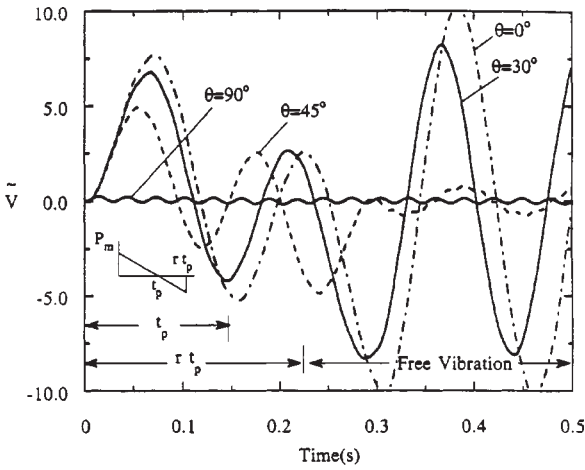
Fig. 3. Influence of ply-angle on time-history of the dimensionless deflection of the beam tip. Sonic-boom overpressure signature. $t_p = 0.15$ s, $r = 1.5$, AR = 16; non-shearable and free-warping beam model.
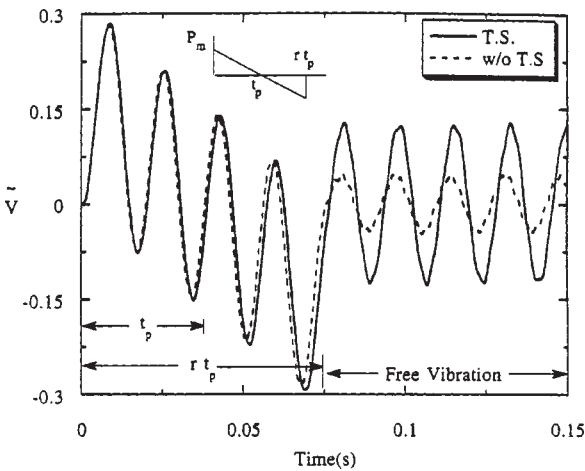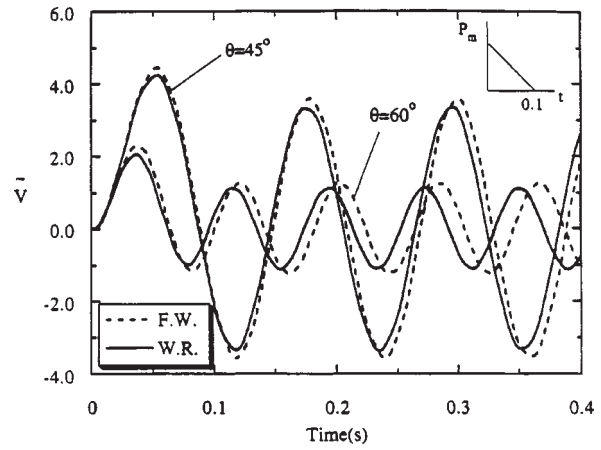

Fig. 5. Influence of the warping restraint and of the ply-angle orientation on time-history of the dimensionless deflection of the beam tip; blast pulse, $t_p = 0.1$ s, $r = 1$, AR = 16, non-shearable beam model.

Fig. 4. Influence of transverse shear on time-history of the dimensionless deflection of the beam tip, sonic boom pulse, $t_p = 0.037$ s, $r = 2$, $\theta = 45°$, AR = 6, free warping model (FW).
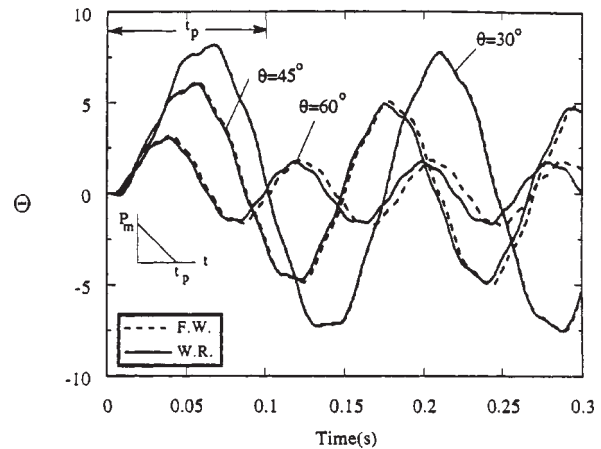

Fig. 6. Influence of the ply-angle and warping restraint on the time-history of the twist of the beam tip; blast pulse, $t_p = 0.1$ s, AR = 16; shearable beam model.

In Figs 5 and 6 the effects of a blast load on the response behavior are displayed. Figure 5 highlights the effect of the ply-angle and of the free and constrained warping models on the dynamic response behavior. The results reveal that while the ply-angle plays a significant role in confining the deflection response, for high aspect ratio beams, as is the case here (AR = 16), the warping inhibition plays a negligible role. At the same time, the results not displayed here, reveal that the classical Euler–Bernoulli counterpart of the case considered in Fig. 5 results in a small increase of the deflection amplitude within both the forced and free motion ranges. In Fig. 6 the time-

history for the twist angle of the beam tip is recorded. This graph highlights the strong effect played by the tailoring technique towards reducing the twist. Figures 7 and 8 record the deflection response of the beam to a rectangular pulse. While in Fig. 7 the effect of the ply-angles is highlighted, in Fig. 8 the effect of transverse shear is displayed. The results in these graphs reveal again the great influence played by the ply-orientation and transverse shear on the transverse deflection response amplitude. The strong influence of transverse shear on deflection amplitude in the free motion range becomes evident also from Fig. 8. Figure 9 displays the transverse deflection response to a step pulse.
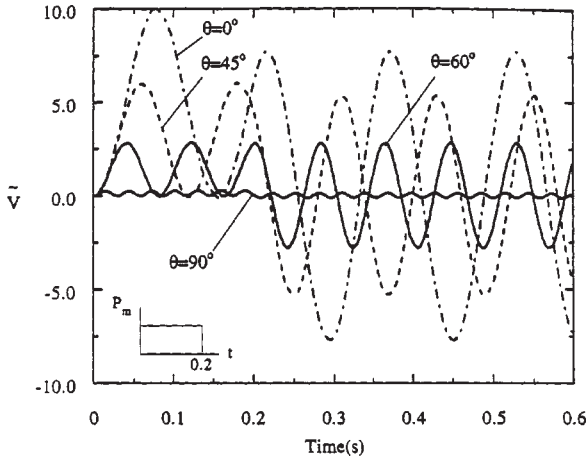
Fig. 7. Influence of the ply-angle on time-history of the dimensionless deflection response of the beam tip, rectangular pulse; $t_p = 0.2$ s, AR = 16, non-sherable and free warping beam models.
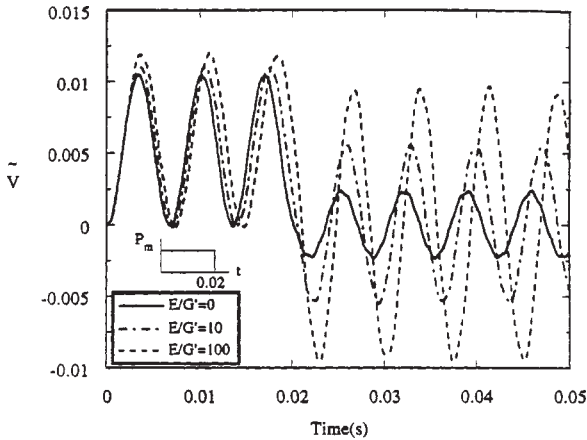

Fig. 8. Influence of transverse shear on time-history of the dimensionless deflection response of the beam tip, rectangular pulse, $t_p = 0.02$ s, AR = 6, warping inhibition included.
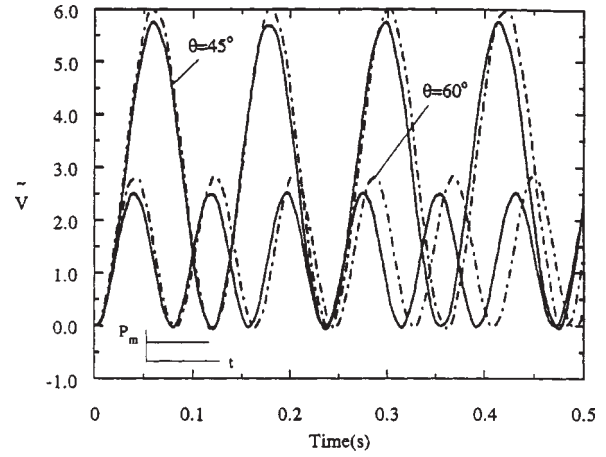

Fig. 9. Influence of ply-angle on time-history of the dimensionless deflection response of the beam tip; step pulse, AR = 16, non-shearable beam model, — · — Free warping; — Warping restraint.
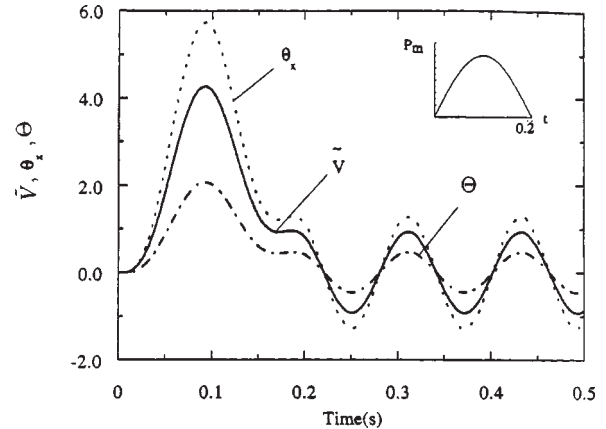

Fig. 10. Dynamic response $(\widetilde{V}, \theta_x$ and $\Theta)$ of the beam tip under a sine pulse, $t_p = 0.2$ s, AR = 16, $\theta = 45°$, shearable and free warping beam model.

In addition to the effect played by the ply-angle, that of the warping restraint emerges clearly from this plot. The results reveal that warping inhibition plays a stronger role in confining the increase of the deflection amplitudes at ply-angles resulting in lower deflection amplitudes. Finally, Fig. 10 displays the dynamic response to a sine pressure pulse. Within this plot the time history of transversal deflection, rotation and twist are presented.

7. Conclusions

In this paper the dynamic response of cantilevered anisotropic thin-walled beams exposed to various time-dependent external pulses has been analyzed, and in this context the effects of the ply-angle, transverse shear, warping restraint and beam aspect ratio have been illustrated. Based on these findings it may be concluded that a consistent evaluation of the time-history structural response of cantilevered thin-walled beams can be accomplished in the framework of a refined structural model incorporating transverse shear and warping inhibition, the latter one being most significant in the case of relatively low aspect ratio beams. The results reveal also the powerful role played by the tailoring technique toward enhancement of the dynamic response of structures exposed to overpressure signatures.

Appendix

The modified local stiffness coefficients K_{ij} ($\equiv K_{ji}$) are:

$$K_{11} = A_{22} - \frac{A_{12}^2}{A_{11}}, \quad K_{12} = A_{26} - \frac{A_{12}A_{16}}{A_{11}},$$

$$K_{13} = 2K_{12}\frac{A_c(z)}{\beta(z)}, \quad K_{14} = B_{22} - \frac{A_{12}B_{12}}{A_{11}},$$

$$K_{22} = A_{66} - \frac{A_{16}^2}{A_{11}}, \quad K_{23} = 2K_{22}\frac{A_c(z)}{\beta(z)},$$

$$K_{24} = B_{26} - \frac{A_{16}B_{12}}{A_{11}}, \quad K_{43} = 2K_{24}\frac{A_c}{\beta},$$

$$K_{44} = D_{22} - \frac{B_{12}^2}{A_{11}}, \quad K_{51} = B_{26} - \frac{B_{16}A_{12}}{A_{11}},$$

$$K_{52} = B_{66} - \frac{B_{16}A_{16}}{A_{11}}, \quad K_{53} = 2K_{52}\frac{A_c}{\beta},$$

$$K_{54} = D_{26} - \frac{B_{12}B_{16}}{A_{11}},$$

where A_{ij}, B_{ij} and D_{ij} are local stretching, bending-stretching and bending stiffness quantitites respectively.

The global stiffness quantities a_{ij} ($\equiv a_{ij}$) and mass coefficients b_i are:

$$a_{33} = \oint \left(K_{11}y^2 - 2yK_{14}\frac{dx}{ds} + K_{44}\left(\frac{dx}{ds}\right)^2 \right)ds,$$

$$a_{37} = \oint \left(yK_{13} - K_{43}\frac{dx}{ds} \right)ds,$$

$$a_{55} = \oint \left(K_{22}\left(\frac{dy}{ds}\right)^2 + A_{44}\left(\frac{dx}{ds}\right)^2 \right)ds,$$

$$a_{56} = -\oint \left(F_\omega K_{21}\frac{dy}{ds} + K_{24}a\frac{dy}{ds} \right)ds,$$

$$a_{66} = \oint \left(K_{11}F_\omega^2 + 2K_{14}F_\omega a + K_{44}a^2 \right)ds,$$

$$a_{77} = \oint 2\frac{A_c}{\beta}K_{23}ds;$$

$$(b_1, b_4, b_{10}) = \oint m_0(1, y^2, F_\omega^2)\,ds;$$

$$(b_{14}, b_{18}) = \oint m_2\left(\left(\frac{dx}{ds}\right)^2, a^2 \right)ds,$$

where

$$(m_0, m_2) = \sum_{k=1}^{N} \int_{h_{(k-1)}}^{h_{(k)}} \rho(k)(1, n^2)\,dn.$$

References

[1] V. Birman and C.W. Bert, Behavior of laminated plates subjected to conventional blast, *Int. J. Impact Eng.* **6**(3) (1987), 145–155.

[2] M.J. Crocker, Multimode response of panels to normal and to travelling sonic booms, *J. Acoust. Soc. Am.* **42** (1967).

[3] M.J. Crocker and R.R. Hudson, Structural response to sonic booms, *J. Sound Vibrations* **9**(3) (1969), 454–468.

[4] J.J. Gottlieb and D.V. Ritzel, Analytical study of sonic boom from supersonic projectiles, *Prog. Aerospace Sci.* **25** (1988), 131–188.

[5] A.D. Gupta, Dynamic analysis of a flat plate subjected to an explosive blast, *Proc. ASME Int. Computers Eng. Conf.* **1** (1985), 491–496.

[6] A.D. Gupta, F.H. Gregory and R.L. Bitting, Dynamic response of a simply supported rectangular plate to an explosive blast, in: *Proc. XIII Southeastern Conf. on Theoretical and Appl. Mech.*, Vol. 1, 1985, pp. 385–390.

[7] R. Houlston, J.E. Slater, N. Pegg and C.G. Des Rochers, On the analysis of structural response of ship panels subjected to air blast loading, *Computer. Struct.* **21** (1985), 273–289.

[8] G. Karpouzian and L. Librescu, A comprehensive model for anisotropic composite aircraft wings suitable for aeroelastic analyses, *J. Aircraft* **31**(3) (1994), 703–712.

[9] L. Librescu and J. Simovich, General formulation for the aeroelastic divergence of composite swept forward wing structures, *J. Aircraft* **25**(4) (1988), 364–371.

[10] L. Librescu and A. Nosier, Response of shear deformable elastic laminated composite flat panels to sonic boom and explosive blast loadings, *AIAA Journal* **28**(2) (1990), 345–352.

[11] L. Librescu and A. Nosier, Dynamic response of anisotropic composite panels to time-dependent external excitations, Paper ICAS-90-1.4R, in: *17th Congress of the International Council of the Aeronautical Sciences*, Stockholm, Sweden, September 1990, pp. 2134–2144.

[12] L. Librescu and S. Thangjitham, Analytical studies on static aeroelastic behavior of forward-swept composite wing structures, *J. Aircraft* **28**(2) (1991), 151–157.

[13] L. Librescu and O. Song, On the static aeroelastic tailoring of composite aircraft swept wings modelled as thin-walled beam structures, *Composites Eng.* **2**(5-7) (Special Issue: *Use of Composites in Rotorcraft and Smart Structures*) (1992), 497–512.

[14] L. Librescu, L. Meirovitch and O. Song, Refined structural modeling for enhancing vibrational and aeroelastic characteristics of composite aircraft wings, *La Recherche Aerospatiale* **1** (1996), 23–35.

[15] L.W. Rehfield and A.R. Atilgan, Toward understanding the tailoring mechanisms for thin-walled composite tubular beams, *Proceedings of the First USSR-U.S. Symposium on Mechanics of Composite Materials*, May 23–26 1989, Riga, Latvia SSR, S.W. Tsai, J.M. Whitney, T.-W. Chou and R.M. Jones, eds, ASME Publ. House, pp. 187–196.

[16] E.C. Smith and I. Chopra, Formulation and evaluation of an analytical model for composite box-beams, *J. Am. Helicopter Soc.* **36**(3) (1991), 23–35.

[17] O. Song and L. Librescu, Free vibration of anisotropic composite thin-walled beams of closed cross-section contour, *J. Sound Vibration* **167**(1) (1993), 129–147.

[18] O. Song and L. Librescu, Bending vibration of cantilevered thin-walled beams subjected to time-dependent external excitations, *J. Acoust. Soc. Am.* **98** (1995), 313–319.

[19] T.A. Weisshaar, Aeroelastic tailoring – creative use of unusual materials, AIAA Paper 87-9076, in: *AIAA/ASME/ASCE/AHS 28th Structures, Structural Dynamics, and Materials Conference*, April 9–10, 1987.